ADVANCED MATERIALS INTERFACES
www.advmatinterfaces.de

On the Question of the Need for a Built-In Potential in Perovskite Solar Cells

Oskar J. Sandberg, Jona Kurpiers, Martin Stolterfoht, Dieter Neher, Paul Meredith, Safa Shoaee, and Ardalan Armin**

Perovskite semiconductors as the active materials in efficient solar cells exhibit free carrier diffusion lengths on the order of microns at low illumination fluxes and many hundreds of nanometers under 1 sun conditions. These lengthscales are significantly larger than typical junction thicknesses, and thus the carrier transport and charge collection should be expected to be diffusion controlled. A consensus along these lines is emerging in the field. However, the question as to whether the built-in potential plays any role is still of matter of some conjecture. This important question using phase-sensitive photocurrent measurements and theoretical device simulations based upon the drift-diffusion framework is addressed. In particular, the role of the built-in electric field and charge-selective transport layers in state-of-the-art p–i–n perovskite solar cells comparing experimental findings and simulation predictions is probed. It is found that while charge collection in the junction does not require a drift field per se, a built-in potential is still needed to avoid the formation of reverse electric fields inside the active layer, and to ensure efficient extraction through the charge transport layers.

1. Introduction

Thin-film solar cells based on perovskite semiconductors have recently exceeded the 25% power-conversion efficiency mark in lab scale devices—approaching crystalline silicon photovoltaics, the market leading technology.[1–3] More broadly, perovskite semiconductors are being intensively studied for use in photodetectors, light-emitting devices and transistors. These semiconductors not only display strong optical absorption and charge generation over a wide and tunable range,[4] but also exhibit high carrier mobilities and long diffusion lengths up to several microns.[5–7] In any light harvesting device, appropriate contacts are critical to efficiently collect the photogenerated charges and deliver them to the external circuit. The contacts are responsible for providing the built-in asymmetry needed to create a driving force for the extraction of photogenerated carriers;[8] this built-in asymmetry can either be established by kinetic selectivity (diffusion-controlled) or by an energetic mismatch (drift-controlled) between the electrodes.

The generic thin-film solar cell is composed of an active layer, sandwiched between a hole-extracting anode contact and an electron-extracting cathode contact. Under illumination, charge carriers generated within the active layer will drift-diffuse to the contacts and be extracted by the built-in asymmetry, resulting in the production of a net photocurrent. In organic solar cells, characterized by low carrier mobilities and short diffusion lengths, a strong built-in electric field across the active layer is necessary to enhance the charge extraction rate and avoid recombination.[9–11] This field is induced by the built-in potential V_{bi} (or contact potential), originating from the work function difference between the anode and cathode and is largely unscreened due to the relatively low dielectric constants of organic semiconductors. Conversely, in perovskite solar cells, exhibiting carrier diffusion lengths of several microns, photogenerated charges should, in the absence of electric fields, be able to effortlessly traverse active layers of 200–500 nm without recombining. Subsequently, provided that kinetic selectivity at the contacts can be ensured,[12] the charge collection is expected to be diffusion controlled,[8,13] and a consensus is emerging along these lines. Kinetic selectivity is established by employing separate charge transport layers (CTLs) in-between the electrodes and the active layer, resulting in either an n–i–p or p–i–n type device architectures, with a hole transport layer (HTL, p-layer) at the anode and an electron transport layer (ETL, n-layer) at the cathode. In the ideal case, these layers are able to conduct majority carriers, while simultaneously preventing the extraction of minority carriers, thus creating a preferred direction for a diffusion-driven charge collection. Within this framework of charge extraction requirements, there is still some conjecture as to the exact role of the in-built potential and hence the precise nature of the driving force responsible for charge extraction.

Dr. O. J. Sandberg, Prof. P. Meredith, Dr. A. Armin
Sustainable Advanced Materials (Sêr-SAM)
Department of Physics
Swansea University
Singleton Park, Swansea, Wales SA2 8PP, UK
E-mail: o.j.sandberg@swansea.ac.uk; ardalan.armin@swansea.ac.uk
Dr. J. Kurpiers, Dr. M. Stolterfoht, Prof. D. Neher, Prof. S. Shoaee
Optoelectronics of Organic Semiconductors
Institute for Physics and Astronomy
University of Potsdam
Potsdam-Golm 14476, Germany
The ORCID identification number(s) for the author(s) of this article can be found under https://doi.org/10.1002/admi.202000041.

DOI: 10.1002/admi.202000041

In this work, we address this question. To this end, a well-established drift-diffusion model is used to investigate the role of built-in potential and contact selectivity in archetypal, high efficiency p–i–n perovskite solar cells (PSCs). To measure the photocurrent, a phase-sensitive AC measurement is employed, which allows for the determination of the photocurrent under forward bias with high precision. The experimental results are interpreted within an analytical framework and compared with numerical predictions. This approach provides robust means to investigate the selectivity of the contacts in operational solar cells.

2. Results

We start by investigating the photocurrent density as a function of the applied voltage of a state-of-the-art p–i–n type perovskite solar cell. For this purpose, we determine the photocurrent in the forward bias with high precision. The photocurrent density is defined by

$$J_{\mathrm{ph}} = J_{\mathrm{light}} - J_{\mathrm{dark}} \tag{1}$$

where J_{light} and J_{dark} are the current densities under illumination and in the dark, respectively. Ideally, the photocurrent is independent of the applied voltage V and is equal to the short-circuit current, $J_{\mathrm{ph}} = -J_{\mathrm{SC}}$, with J_{SC} being the magnitude of the short-circuit current density. In general, however, $J_{\mathrm{ph}}(V)$ is determined by the interplay between charge carrier recombination and collection, which is ultimately governed by the properties of the contacts and the prevailing driving force for extraction.[14–18]

Experimentally, the photocurrent is often taken as the difference between the total current under illumination and in the dark, in accordance with Equation (1). However, this approach becomes unreliable at forward-bias voltages above 1 V because of device heating effects.[19] In addition, PSCs usually also suffer from current–voltage hysteresis caused by ion-induced redistribution of the electric field,[20] which generally depends on the prevailing illumination level. These issues can be avoided by the use of a perturbative phase-sensitive method, as employed in this work, which allows us to measure photocurrents orders of magnitude smaller than the total current which would otherwise not be detectable in conventional DC measurements. The experimental set up used for the phase-sensitive measurements is illustrated in **Figure 1**. Further details regarding the experimental technique and the device fabrication are given in the Experimental Section.

Figure 2a,b shows, respectively, the experimental current density–voltage (J–V) characteristics and the corresponding normalized J_{ph}–V curves, as obtained from low-light intensity AC measurements, of the perovskite solar cell. For comparison, we also included an organic bulk heterojunction solar cell based on PCDTBT (poly[N-9′-heptadecanyl-2,7-carbazole-alt-5,5-(4′,7′-di-2-thienyl-2′,1′,3′-benzothiadiazole)]) and PCBM ([6,6]-Phenyl-C71-butyric acid methyl ester). The organic solar cell (ITO/MoO_3/PCDTBT:PCBM/Ca/Al device structure) shows a reversal of the photocurrent at voltages close to the built-in potential (expected to be around 1.0 V in these device structures). This behavior has previously been assigned to the reversed polarity of the internal electric field, and subsequent reversed direction of charge extraction,[14–18] consistent with a metal–intrinsic semiconductor–metal (m–i–m) structure.[21,22] In contrast, the photocurrent of the perovskite solar cell remains negative for voltages far into the forward bias.

To investigate the role of the selective transport layers we fabricated p–i–n PSCs with different types of HTLs and ETLs. The corresponding experimental results for the J–V and the normalized J_{ph}–V curves are shown, respectively, in Figure 2c,d. At low voltages, the photocurrent is essentially identical to the total current obtained under illumination. At higher voltages, different behaviors for the different devices can, however, be distinguished. For the case without an HTL, the photocurrent changes its sign at a relatively low voltage of roughly 1 V. This is fully consistent with an expected increased surface recombination at the anode contact, as also evident from the reduced open-circuit voltage (V_{oc}). By inserting an HTL of polyTPD (poly[*N*,*N*′-bis(4-butylphenyl)-N,N′-bisphenylbenzidine]) at the anode, an increase in the V_{oc} of ≈0.3 V is obtained. This observation suggests that a drastic reduction in the surface recombination of electrons at the anode takes place using polyTPD as an HTL. Furthermore, the photocurrent remains negative for voltages far into the forward bias region and well above the V_{oc}

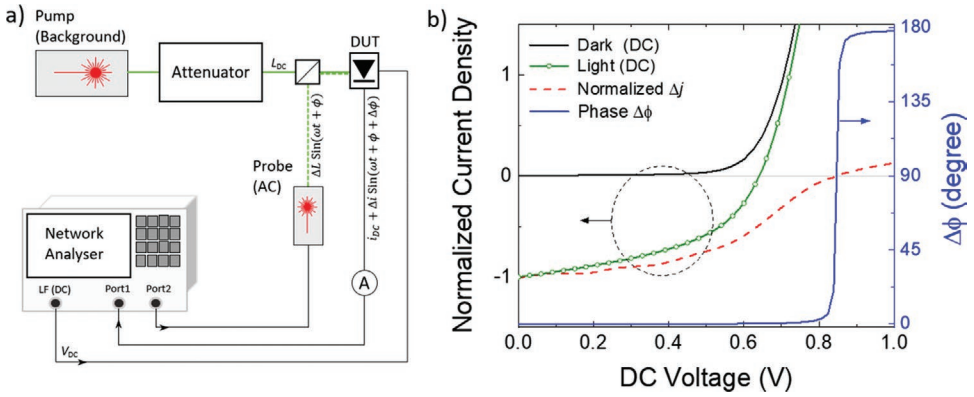

Figure 1. a) Schematic of the experimental setup for the phase-sensitive AC measurement of photocurrent where DUT is the device under test. The DUT is pumped with attenuated DC illumination and addressed with a secondary AC probe generating an additional current Δj. b) The corresponding photocurrent density (red dashed line) and phase (blue line) of the AC photocurrent.

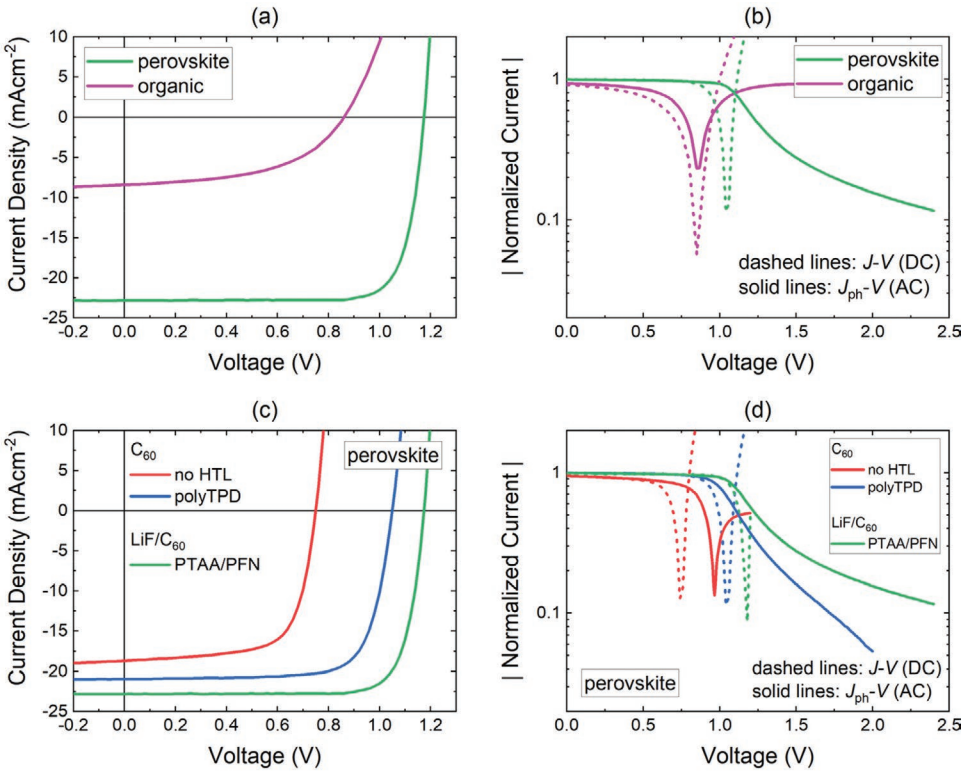

Figure 2. Experimental *J–V* curves at 1 sun incident light intensity a) and the corresponding normalized photocurrents b) for a state-of-the-art p–i–n type perovskite solar cell with hole transport layer of PTAA/PFN and electron transport layer of LiF/C_{60}. For comparison, an organic solar cell based on ITO/MoO_3/PCDTBT:PCBM/Ca/Al has been included. In c,d), the corresponding current–voltage characteristics and normalized photocurrents for perovskite solar cells with different hole transport layers (HTLs—polyTPD or PTAA/PFN) and electron transport layers (ETLs—C_{60} or LiF/C_{60}) are shown.

and the built-in potential (we note the maximum V_{bi} is equal to the bandgap of the absorber layer divided by the elementary charge q). Finally, a similar behavior can also be seen for the state-of-the-art planar PSC, using PTAA (poly[bis(4-phenyl)(2,4,6-trimethylphenyl)amine]) and PFN (poly({9,9-bis[30-({N,N-dimethyl}-N-ethylammonium)-propyl]-2,7-fluorene}-alt-2,7-{9,9-di-n-octylfluorene})) for the HTL and LiF/C_{60} as the ETL:PTAA/PFN/perovskite/LiF/C_{60},[23] which exhibits the largest open-circuit voltage (1.18 V) and the highest power conversion efficiency of the three (up to ≈21.5%). Notably, the photocurrent remains negative well above 2 V.

In order to understand the observed behavior in more detail, we performed numerical simulations based on a drift-diffusion model on the perovskite device. In this model, the charge-transport layers are assumed to be composed of undoped organic semiconductors, forming large energetic barriers for minority carriers at the CTL/active layer interfaces. We note that in many cases the charge transport layers are also doped, however, this is generally expected to increase interfacial recombination between majority carriers in the interlayer and minority carriers in the active layer. In our model, the interface recombination at the CTL/active layer is assumed to be negligible. The recombination within the active layer is assumed to be bimolecular; we note that including trap-assisted recombination in the active layer did not change the qualitative behavior of the simulations and was therefore omitted. Furthermore, a uniform charge carrier generation rate and balanced mobilities (μ_{AL}) of 10 $cm^2\ V^{-1}\ s^{-1}$ for electrons and holes are assumed in the perovskite active layer, whereas a hole mobility of 10^{-3} $cm^2\ V^{-1}\ s^{-1}$ in the HTL and an electron mobility of 1 $cm^2\ V^{-1}\ s^{-1}$ in the ETL is implemented. These mobility values are within a reasonable range for typical materials used in perovskite solar cells.[7,23–25] We note that from a qualitative perspective, however, the results remain agnostic to small changes to these values. The details of the drift-diffusion model are given in the Supporting Information.

Figure 3 shows the simulated *J–V* curves, and the corresponding J_{ph}–*V* for a p–i–n type perovskite solar cell. Note that in the numerical calculations, J_{ph} is obtained using Equation (1). For comparison, we also simulated the case with a m–i–m type structure, corresponding to a situation without (or very leaky) CTLs. It can be seen that the simulations are able to reproduce the experimental behavior seen in Figure 2c,d. Upon comparing the p–i–n and the m–i–m devices in Figure 3 with each other, the importance of the CTLs is readily visible. Most notably, the absence of CTLs is manifested by a decrease in the open-circuit voltage. Furthermore, while the m–i–m device shows a reversal of the photocurrents at $V \leq V_{bi}$, after introducing charge-selective CTLs (p–i–n) the photocurrent remains negative far into the forward-bias well above V_{bi}. It should be noted that ionic effects[20,26,27] have been neglected in these simulations.

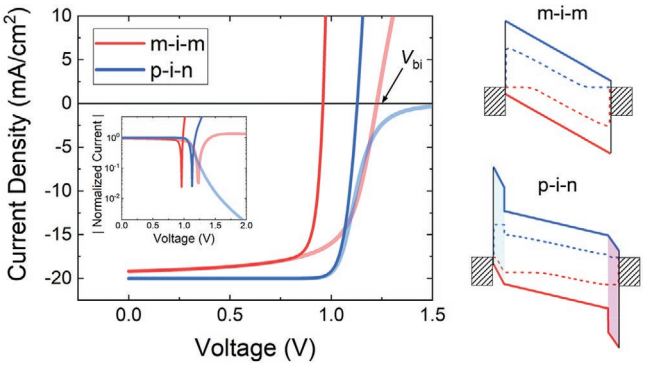

Figure 3. Simulated current density-voltage characteristics (dark lines) and photocurrent (lightly colored lines) at 1 sun light intensity for a perovskite solar cell with (p–i–n) and without (m–i–m) CTLs. The corresponding normalized currents are shown on a log-line plot in the inset to the left. A built-in potential (electrode work function difference) of V_{bi} = 1.25 V is assumed for both cases. The insets to the right show the corresponding band diagrams simulated under short-circuit conditions (under illumination); the conduction (valence) band edge E_c (E_v) is depicted by the blue (red) solid line, whereas the electron (hole) quasi-Fermi level E_{Fn} (E_{Fp}) is depicted by the blue (red) dashed line.

For the m–i–m device, the photocurrent behavior and the decreased open-circuit voltage can be attributed to an increased surface recombination of minority carriers at the active layer/electrode contacts, taking place at voltages below V_{bi}, even though a considerable electric field is present in the active layer. This is a consequence of the high mobilities of electrons and holes within the perovskite active layer, resulting in a non-negligible amount of both photogenerated and injected carriers diffusing against the electric field and being collected at the "wrong" electrode.[28–30] Close to $V = V_{bi}$, flat-band conditions are established, and the charge extraction is solely driven by diffusion, but because of the nonselective contacts, any extraction current of electrons is balanced by an equal but opposite surface recombination current of holes. Upon further increasing the voltage beyond this point, the direction of the photocurrent is reversed. Subsequently, the built-in potential sets the upper limit for both the photocurrent reversal voltage and the open-circuit voltage in the case of nonselective (metal-like) contacts.

The situation is markedly different for the p–i–n device. First, owing to the large extraction barriers for minority carriers at the CTL/active layer interfaces, the surface recombination of minority carriers at the electrode contacts is expected to be negligible. Under these conditions, the open-circuit voltage is determined by the recombination inside the active layer and its interfaces only. Second, because the CTLs are composed of intrinsic organic semiconductors, exhibiting much lower relative permittivity (ε = 3–4) compared to the perovskite active layer (here, assumed to be ε = 24[31]), a significant portion of the built-in potential will drop across the CTLs under short-circuit conditions. If we assume uniform built-in electric fields $F_j = -V_{bi,j}/L_j$ inside each layer j (the space charge density being negligible), the reduced built-in potential across the active layer (AL) is then given by

$$V_{bi,AL} = V_{bi} \times \frac{C_{AL}^{-1}}{C_{HTL}^{-1} + C_{AL}^{-1} + C_{ETL}^{-1}} \quad (2)$$

where $C_j = \varepsilon_j \varepsilon_0 / L_j$ is the geometric capacitance of layer j (where j = HTL, AL, ETL). Analogous expressions are valid for the built-in potential differences across the other layers. We therefore expect the electric field strengths to be high within the CTLs, while a notably smaller built-in field is present within the perovskite active layer compared to the m–i–m case.

As noted above, apart from an increased open-circuit voltage (relative to the m–i–m case), the p–i–n device also exhibits a distinctly different photocurrent behavior, with the photocurrent remaining negative for voltages well above the built-in potential. This suggests that photogenerated carriers are diffusing against the electric field at very high forward-bias voltages, even though the electric field is strongly reversed. We note that the actual magnitude of the photocurrent for $V > V_{OC}$ is strongly dependent on both the dominating bulk recombination mechanism and its strength. Because of the large mobilities in the active layer, the diffusion lengths of electrons and holes are expected to be much larger than the active layer thickness. This seems to imply that a built-in electric field is not necessary to drive photogenerated charge carriers inside the perovskite layer towards their respective CTLs, as long as the contacts remain selective. To further investigate the role of the built-in potential on the charge extraction in perovskite solar cells, its effect on the photocurrent is simulated in **Figure 4**a. By decreasing V_{bi} a drastic decrease of the device performance is obtained. Note that the open-circuit voltage remains, in principle and in the absence of shunts, fixed at 1.12 V, independent of V_{bi}; as expected for the case with selective contacts.[32]

Figure 4b shows the simulated J–V curves for the case with a low built-in potential of V_{bi} = 0.45 V. The corresponding band diagrams at short circuit and close to open circuit, respectively, are simulated in Figure 4c,d. As evident from Figure 4d, the potential drop across the active layer will be close to zero for voltages $V > V_{bi}$. Subsequently, the photogenerated carriers inside the active layer are driven by diffusion under these conditions. Because the contacts are selective, photogenerated electrons, and holes will diffuse toward the ETL and the HTL, respectively. This diffusion of photogenerated carriers is competing with the recombination of photogenerated carriers with injected charge carriers from the contacts. Conversely, almost all of the potential drops across the CTLs, because of their small dielectric constants. This effect is particularly prominent for CTLs with conductivities much smaller than that of the active layer (under solar cell operating conditions). As a result, the electric fields within the CTLs are reversed, opposing the extraction of majority carriers—as we see experimentally.

To gain more insight, we consider the following simplified analytical description for the case when the HTL limits the charge collection. For simplicity, we assume a constant recombination lifetime τ for carriers in the active layer and take the electric field to be zero in this layer (the entire potential drops across the CTLs). Then, assuming the interface recombination to be negligible (selective CTLs) and taking the carrier diffusion length to be much larger than the active layer thickness ($(\mu_{AL} \tau kT/q)^{1/2} \gg L_{AL}$), the photocurrent can be approximated as

$$J_{ph} \approx -J_{gen} \times \left[1 + \frac{\tau_{col}}{\tau}\right]^{-1} \quad (3)$$

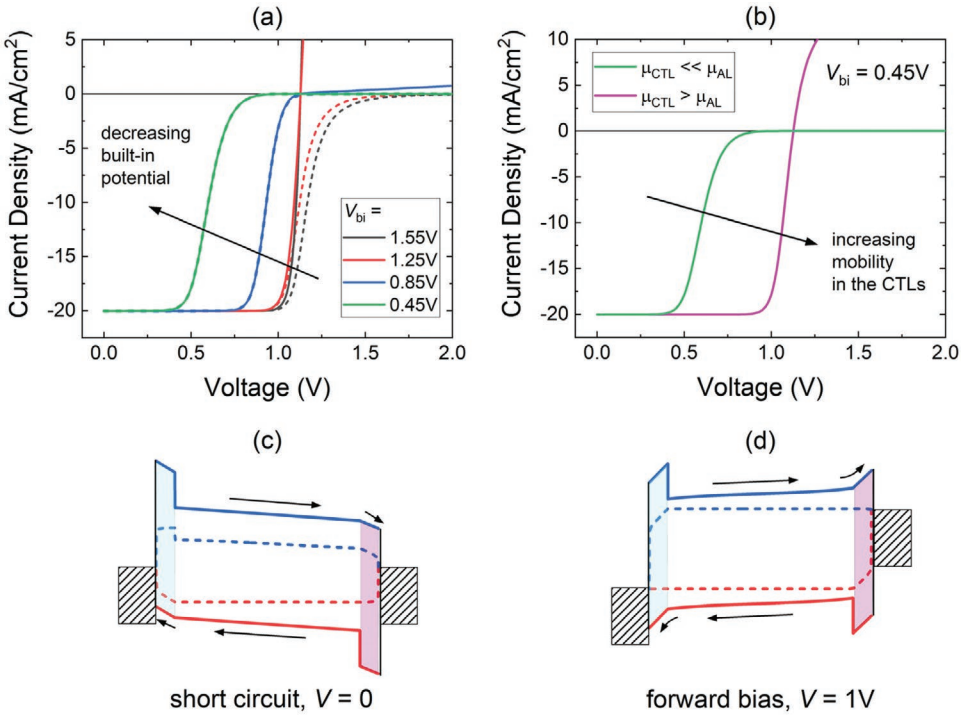

Figure 4. a) Simulated current–voltage characteristics (solid lines) and photocurrent (dashed lines) at 1 sun light intensity for a p–i–n perovskite solar cell for varying built-in potentials. b) The current–voltage characteristics for a p–i–n perovskite solar cell at a V_{bi} = 0.45 V, showing a significant improvement when the mobilities in the CTLs are increased from $\mu_{ETL} = 0.1\mu_{AL}$ and $\mu_{HTL} = 0.01\mu_{AL}$ ("$\mu_{CTL} \ll \mu_{AL}$") to $\mu_{ETL} = \mu_{HTL} = 10\mu_{AL}$ ("$\mu_{CTL} > \mu_{AL}$"). In c,d), the corresponding band diagrams for the case V_{bi} = 0.45 V under short-circuit conditions (under illumination) and in forward bias for $V > V_{bi}$ are shown (for "$\mu_{CTL} \ll \mu_{AL}$").

as shown in the Supporting Information. Here, J_{gen} is the magnitude of the total photogeneration current density, whereas

$$\tau_{col} = \frac{L_{AL}L_{HTL}}{\mu_{HTL}U_{HTL}} \times \left[1 - \exp\left(-\frac{qU_{HTL}}{kT}\right)\right] \quad (4)$$

is the effective extraction time for holes collected via the HTL. U_{HTL} is the potential difference across the HTL, becoming negative for $V \gg V_{bi}$ when the electric field in the HTL is reversed, while kT/q is the thermal voltage. Note that $\tau_{col} = qL_{AL}L_{HTL}/\mu_{HTL}kT$ at flat-band conditions ($U_{HTL} = 0$).

In accordance with Equation (3), the photocurrent collection is determined by the competition between carrier recombination (of rate τ^{-1}) in the active layer and the carrier extraction via the HTL (with rate τ_{col}^{-1}). At small voltages ($U_{HTL} \gg kT/q$), the extraction rate is dominant. When $V \gg V_{bi}$, in turn, the electric field in the HTL is reversed ($U_{HTL} < 0$). Subsequently, holes have to diffuse against the electric field in order to be collected at the anode; this is manifested by an exponentially increasing τ_{col} with voltage. At strong reverse electric fields, the diffusion time for holes to traverse the HTL is much longer than the bulk recombination lifetime in the active layer, $\tau_{col} \gg \tau$, and the photogenerated charge carriers in the active layer "waiting to be extracted" are inevitably lost.

These findings suggest that a large enough V_{bi} is needed to ensure a sufficient driving force for the extraction of majority carriers within the CTLs. This limitation can be partly relaxed by increasing the mobility of the transport layers. This is demonstrated in Figure 4b, where we included the case with a significantly increased mobility of the HTL and ETL, showing a drastic improvement of the fill factor. In general, the transport losses in the CTLs can also be reduced by increasing the conductivity of the charge-transport layers through doping.[33] Subsequently, the necessary condition for the HTL not to limit the majority carrier (hole) extraction current (J_{maj}) may be expressed as $J_{SC} < J_{maj} \sim qp_{HTL}L_{AL}/\tau_{col}$, where p_{HTL} is the hole density in the HTL. In the case of a highly conductive transport layer, the work function of the contact is thus less important, provided that sufficient selectivity can be assured.[34]

Note that we have assumed matched energy levels for majority carriers at the CTL/active layer interfaces. However, the carrier density, and thus the conductivity, of the CTL can also be increased by increasing the energetic injection barrier ΔE_{maj} for majority carriers at the CTL/active layer interface. This leads to an exponential increase of the majority carrier density within the charge-transport layer ($p_{HTL} \propto \exp(\Delta E_{maj}/kT)$). However, if a considerable amount of interface states is present at the CTL/active layer interface in question, an increase in ΔE_{maj} leads to a corresponding exponential increase of surface recombination at this interface as well (which outweighs the benefits due to the increased carrier density in the HTL), resulting in increased V_{oc} losses.[23,35]

We also investigated the impact of the energetic barrier for the extraction of minority carriers at the CTL/active layer interfaces. The J–V curves and photocurrents at different extraction barriers for minority carriers (ΔE_{min}^{HTL}) at the HTL/active layer

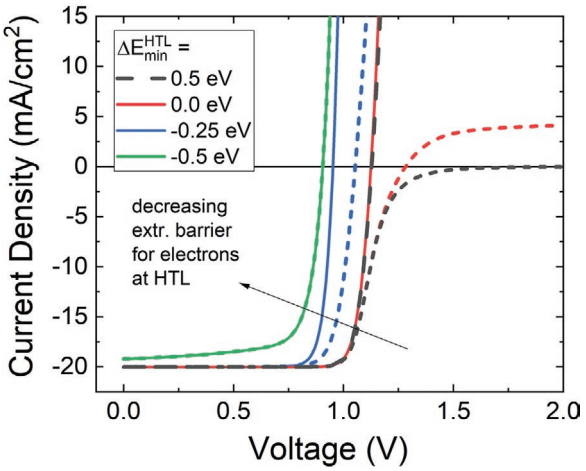

Figure 5. Simulated current–voltage characteristics (solid lines) and photocurrent (dashed lines) at 1 sun light intensity for p–i–n perovskite solar cells with different electron extraction barriers at the HTL/active layer interface. The electron and hole mobilities within the HTL are equal at 10^{-3} cm^2 V^{-1} s^{-1}. The anode work function is assumed fixed (relative to the band edges in the active layer), and V_{bi} = 1.25 V.

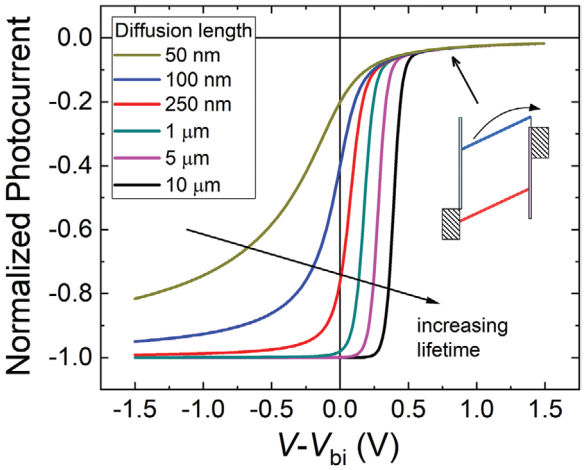

Figure 6. The normalized photocurrent versus the internal potential difference $V - V_{bi}$ inside the active layer based on an analytical model (Equation S15, Supporting Information), assuming idealized metallic, but perfectly selective CTLs, for varying carrier diffusion lengths inside the perovskite layer. The electric field inside the active layer is assumed uniform and given by $F = (V - V_{bi})/L_{AL}$, where $V - V_{bi} = 0$ corresponds to flat-band conditions ($F = 0$). A carrier mobility of 10 cm^2 V^{-1} s^{-1} and thickness of 250 nm are assumed for the active layer.

interface is simulated in **Figure 5**. It can be seen that, provided V_{bi} is large enough, the presence of a large ΔE_{min}^{HTL} is less important. In fact, under relevant solar cell operating conditions, an equal device performance is obtained for the case with no barrier ($\Delta E_{min}^{HTL} = 0$) as with a large barrier for minority carrier extraction ($\Delta E_{min}^{HTL} = 0.5$ eV), consistent with previous studies.[23] This is because i) the low minority carrier mobility in the CTLs acts as a kinetic barrier for the extraction of minority carriers, and ii) the reverse electric field in the CTLs further prevents the unintentional diffusion of minority carriers through the CTL. The recombination at the HTL/active layer interface becomes significant only at higher voltages, above the open-circuit voltage, as manifest through the reversal of the photocurrent. We note, however, that in case of CTLs with high minority carrier mobilities, the condition i) is no longer valid and a large energetic barrier at the CTL/active layer is essential to avoid surface recombination at the electrodes. As the ΔE_{min}^{HTL} is reduced below zero, a drastic increase of the recombination at the HTL/active layer interface is obtained, resulting in substantial V_{oc} losses. Furthermore, as a consequence of the drastically increased interface recombination, which is attributed to the increased hole density within the HTL, the photocurrent changes sign at voltages well below the built-in potential. In this limit, the HTL is effectively behaving more and more like a metal.

Based on the above considerations, it is clear that a high V_{bi} is needed to avoid transport-limitations in the CTLs while simultaneously avoiding increased interface recombination. To answer the question of whether the perovskite active layer itself needs a high V_{bi} to operate efficiently under solar cell operating conditions, we finally consider the idealized case with transport layers that are highly conductive (metallic) yet remain perfectly selective at all times. To explicitly clarify the role of the internal electric field, we investigate a perovskite layer with a uniform electric field $F = (V - V_{bi})/L_{AL}$ and constant recombination lifetime τ and diffusion length $L_n = (\mu\tau kT/q)^{1/2}$ for electrons. Under these simplified conditions, the transport equations can again be solved analytically (see Supporting Information). The corresponding normalized photocurrents for different diffusion lengths are shown in **Figure 6**. It can be seen that for diffusion lengths much larger than the active layer thickness, the charge collection in the absence of an electric field ($V - V_{bi} = 0$) is efficient, as expected. This suggests that field-free regions within the active layer, e.g., caused by ionic screening effects, are not detrimental to the device performance, provided that the carrier diffusion lengths are much larger than the active layer thickness.

Although the charge carrier extraction from the active layer can be efficient in the absence of an electric field, Figure 6 clearly demonstrates that a high enough V_{bi} is crucial in order to avoid charge collection losses occurring at $V > V_{bi}$, corresponding to a voltage regime where the electric field changes polarity. In this field-reversed regime, the photogenerated electrons are driven toward and accumulate at the (electron-blocking) HTL. To reach the ETL, the electrons have to diffuse against the reversed electric field, posing as an effective extraction barrier of height $q(V - V_{bi})$. This significantly increases the average time it takes for carriers to be extracted with increasing applied voltage, ultimately giving more time for carriers to recombine inside the active layer. Note that similar qualitative behavior is expected to apply when ionic screening effects are taken into account; although the electric field inside the active layer is largely screened in this case, the effective extraction barrier $q(V - V_{bi})$ is instead formed across ionic space charge regions. We emphasize that this analysis assumes perfectly selective CTLs and thus neglects the interface recombination which would otherwise be significantly enhanced in the field-reversed regime when minority carriers are pushed against the interfaces, making the necessity of a high enough V_{bi}, such that $V_{bi} > V_{oc}$, in perovskite solar cells even more important.

3. Conclusions

In summary, we have investigated the effect of the built-in potential on the photocurrent collection in perovskite solar cells. We find that, for the case of undoped organic charge-transport layers, the majority carrier mobility of the organic interlayers limits the driving force for photocurrent generation in p–i–n structures with low built-in potentials. Furthermore, even in the presence of optimized charge transport layers, a low built-in potential might also give rise to a reversed electric field inside the perovskite active layer under operating conditions increasing the recombination of the photogenerated charge carriers inside the said layer. Our findings emphasize the necessity of a high enough electrode work function difference in perovskite solar cells to both ensure efficient extraction of majority carriers within the charge transport layers and avoid the reversal of the electric field inside the active layer under solar cell operating conditions. Our approach has general utility in examining contact dynamics in not only solar cells but other optoelectronic systems as well, and we note it may be particularly useful in the context of 2D–3D perovskites to study transport through the 2D capping layer.

4. Experimental Section

Device Fabrication: Prepatterned 2.5 × 2.5 cm^2 15 Ω sq^{-1} ITO (Automatic Research, Germany), glass or fused silica substrates were cleaned with acetone, 3% Hellmanex solution, DI water, and isopropanol, by sonication for 10 min in each solution. After a microwave plasma treatment (4 min, 200 W), the samples were transferred to an N_2-filled glovebox where different CTLs were spin coated from solution. Bottom selective contacts (HTLs or ETLs): PolyTPD (Ossila) was spin coated from a 1.5 mg mL^{-1} DCB solution at 6000 rpm for 30 s (acceleration 2000 rpm s^{-1}) and subsequently annealed 100 °C for 10 min. PTAA (Sigma Aldrich) was spin coated from a 1.5 mg mL^{-1} Toluene solution at 6000 rpm for 30 s (acceleration 2000 rpm s^{-1}) and subsequently annealed 100 °C for 10 min. For PTAA coated samples, a 60 µL solution of PFN-P2 (0.5 mg mL^{-1} in methanol) was added onto the spinning substrate at 5000 rpm for 20 s resulting in a film with a thickness below the detection limit of our AFM (<5 nm).

Perovskite Layer: The triple cation perovskite solution was prepared by mixing two 1.3 M FAPbI3 and MAPbBr3 perovskite solutions in DMF:DMSO (4:1) in a ratio of 83:17 which is called the "MAFA" solution. The 1.3 M FAPbI3 solution was thereby prepared by dissolving FAI (722 mg) and PbI_2 (2130 mg) in 2.8 mL DMF and 0.7 mL DMSO (note there is a 10% excess of PbI_2). The 1.3 M $MAPbBr_3$ solution was made by dissolving MABr (470 mg) and $PbBr_2$ (1696 mg) in 2.8 mL DMF and 0.7 mL DMSO (note there is a 10% excess of $PbBr_2$). Last, 40 µL of a 1.2 M CsI solution in DMSO (389 mg CsI in 1 mL DMSO) was mixed with 960 µL of the MAFA solution resulting in a final perovskite stoichiometry of $(CsPbI_3)_{0.05}[(FAPbI_3)_{0.83}(MAPbBr_3)_{0.17}]_{0.95}$ in solution. The perovskite film was deposited by spin coating at 4000 rpm (acceleration 1300 rpm s^{-1}) for 35 s; 10 s after the start of the spinning process, the spinning substrate was washed with 300 µL EA for ≈1 s (the antisolvent was placed in the center of the film). The perovskite film was then annealed at 100 °C for 1 h on a preheated hotplate.

Top selective contacts (HTLs or ETLs): For C_{60} (Creaphys) and LiF ETLs, the perovskite films were transferred to an evaporation chamber where 30 nm of C_{60} (1 nm of LiF) were deposited at 0.1 Å s^{-1} (0.03 Å s^{-1}) under vacuum (10^{-7} mbar).

Metal Contacts: p-i-n devices were completed by transferring the samples to an evaporation chamber where 8 nm BCP (Sigma-Aldrich) at 0.2 Å s^{-1} and 100 nm copper (Sigma-Aldrich) at 0.6 Å s^{-1} were deposited under vacuum (10^{-7} mbar).

Current–Voltage Characteristics: *J–V* curves were measured under N_2 on a Keithley 2400 system in a two-wire configuration with a scan speed of 0.1 V s^{-1} and voltage step of 0.02 V. One sun illumination at ≈100 mW cm^{-2} of AM1.5G irradiation was provided by an Oriel class ABA solar simulator. The real illumination intensity was monitored during the measurement using a Si photodiode and the exact illumination intensity was used for efficiency calculations. The sun simulator was calibrated with a KG5 filtered silicon solar cell (certified by Fraunhofer ISE). The AM1.5G short-circuit current of devices matched the integrated product of the EQE spectrum within 5–10% error. The latter was recorded using a home-built set-up utilizing a Philips Projection Lamp (Type7724 12 V 100 W) in front of a monochromator (Oriel Cornerstone 74100) and the light was mechanically chopped at 70 Hz. The photogenerated current was measured using a lock-in-amplifier (EG&G Princeton Applied Research Model 5302, integration time 300 ms) and evaluated after calibrating the lamp spectrum with a UV-enhanced Si photodetector (calibrated at Newport).

Photocurrent Measurements: A schematic picture of the experimental measurement setup is shown in Figure 1a. Using a KEYSIGHT E5061B network analyzer (NA), the S parameter was used; the S-parameter was expressed as the magnitude and phase pairs, in a log magnitude format. The S-parameter was used to measure the magnitude and phase of the transmitted power signal, from an LED to our solar cell while applying a bias sweep. A Stanford research system (SR570) amplifier was used in conjunction for tuning of the LED's power. A pump (CrystaLaser Nordic Combiner) provided the background recombination level (for instance the 1 Sun condition).

Supporting Information

Supporting Information is available from the Wiley Online Library or from the author.

Acknowledgements

This work was supported by the Sêr Cymru Program through the European Regional Development Fund, Welsh European Funding Office and Swansea University strategic initiative in Sustainable Advanced Materials. S.S and J.K. acknowledge Alexander von Humboldt Foundation for funding. The authors thank Seyed Mehrdad Hosseini for providing the PCDTBT:PCBM device. A.A. is a Sêr Cymru II Rising Star Fellow and P.M. a Sêr Cymru II National Research Chair.

Conflict of Interest

The authors declare no conflict of interest.

Keywords

built-in potential, charge collection, charge transport layers, perovskite solar cells

Received: January 8, 2020
Revised: February 15, 2020
Published online:

[1] M. A. Green, E. D. Dunlop, D. H. Levi, J. Hohl-Ebinger, M. Yoshita, A. W. Y. Ho-Baillie, *Prog. Photovoltaics* **2019**, *27*, 565.
[2] J.-P. Correa-Baena, M. Saliba, T. Buonassisi, M. Grätzel, A. Abate, W. Tress, A. Hagfeldt, *Science* **2017**, *358*, 739.

[3] W. Tress, *Adv. Energy Mater.* **2017**, *7*, 1602358.
[4] G. Hodes, *Science* **2013**, *342*, 317.
[5] Q. Dong, Y. Fang, Y. Shao, P. Mulligan, J. Qiu, L. Cao, J. Huang, *Science* **2015**, *347*, 967.
[6] S. D. Stranks, G. E. Eperon, G. Grancini, C. Menelaou, M. J. P. Alcocer, T. Leijtens, L. M. Herz, A. Petrozza, H. J. Snaith, *Science* **2013**, *342*, 341.
[7] T. Kirchartz, L. Kruckemeier, E. L. Unger, *APL Mater.* **2018**, *6*, 100702.
[8] P. Würfel, *Physics of Solar Cells*, 2nd ed., Wiley-VCH, Weinheim, Germany **2009**.
[9] C. Deibel, V. Dyakonov, *Rep. Prog. Phys.* **2010**, *73*, 096401.
[10] D. Bartesaghi, I. del Carmen Pérez, J. Kniepert, S. Roland, M. Turbiez, D. Neher, L. J. A. Koster, *Nat. Commun.* **2015**, *6*, 7083.
[11] D. Neher, J. Kniepert, A. Elimelech, L. J. A. Koster, *Sci. Rep.* **2016**, *6*, 24861.
[12] E. J. Juarez-Perez, M. Wussler, F. Fabregat-Santiago, K. Lakus-Wollny, E. Mankel, T. Mayer, W. Jaegermann, I. Mora-Sero, *J. Phys. Chem. Lett.* **2014**, *5*, 680.
[13] T. Kirchartz, J. Bisquert, I. Mora-Sero, G. Garcia-Belmonte, *Phys. Chem. Chem. Phys.* **2015**, *17*, 4007.
[14] M. Limpinsel, A. Wagenpfahl, M. Mingebach, C. Deibel, V. Dyakonov, *Phys. Rev. B* **2010**, *81*, 085203.
[15] A. Petersen, T. Kirchartz, T. A. Wagner, *Phys. Rev. B* **2012**, *85*, 045208.
[16] D. J. Wehenkel, L. J. A. Koster, M. M. Wienk, R. A. J. Janssen, *Phys. Rev. B* **2012**, *85*, 125203.
[17] R. Sokel, R. C. Hughes, *J. Appl. Phys.* **1982**, *53*, 7414.
[18] O. J. Sandberg, M. Nyman, R. Österbacka, *Phys. Rev. Appl.* **2014**, *1*, 024003.
[19] Z. E. Ooi, R. Jin, J. Huang, Y. F. Loo, A. Sellinger, J. C. deMello, *J. Mater. Chem.* **2008**, *18*, 1644.
[20] Y. Zhang, M. Liu, G. E. Eperon, T. C. Leijtens, D. McMeekin, M. Saliba, W. Zhang, M. de Bastiani, A. Petrozza, L. M. Herz, M. B. Johnston, H. Lin, H. J. Snaith, *Mater. Horiz.* **2015**, *2*, 315.
[21] P. W. M. Blom, V. D. Mihailetchi, L. J. A. Koster, D. E. Markov, *Adv. Mater.* **2007**, *19*, 1551.
[22] D. Rauh, A. Wagenpfahl, C. Deibel, V. Dyakonov, *Appl. Phys. Lett.* **2011**, *98*, 133301.
[23] M. Stolterfoht, P. Caprioglio, C. M. Wolff, J. A. M. Prieto, J. Nordmann, S. Zhang, D. Rothhardt, U. Hörmann, Y. Amir, A. Redinger, L. Kegelmann, F. Zu, S. Albrecht, N. Koch, T. Kirchartz, M. Saliba, T. Unold, D. Neher, *Energy Environ. Sci.* **2019**, *12*, 2778.
[24] T. S. Sherkar, C. Momblona, L. Gil-Escrig, H. J. Bolink, L. J. A. Koster, *Adv. Energy Mater.* **2017**, *7*, 1602432.
[25] Q. Burlingame, C. Coburn, X. Che, A. Panda, Y. Qu, S. R. Forrest, *Nature* **2018**, *554*, 77.
[26] P. Calado, A. M. Telford, D. Bryant, X. Li, J. Nelson, B. C. O'Regan, P. R. F. Barnes, *Nat. Commun.* **2016**, *7*, 13831.
[27] D. Moia, I. Gelmetti, P. Calado, W. Fisher, M. Stringer, O. Game, Y. Hu, P. Docampo, D. Lidzey, E. Palomares, J. Nelson, P. R. F. Barnes, *Energy Environ. Sci.* **2019**, *12*, 1296.
[28] W. Tress, K. Leo, M. Riede, *Phys. Rev. B* **2012**, *85*, 155201.
[29] O. J. Sandberg, A. Sundqvist, M. Nyman, R. Österbacka, *Phys. Rev. Appl.* **2016**, *5*, 044005.
[30] O. J. Sandberg, A. Armin, *Synth. Met.* **2019**, *254*, 114.
[31] F. Brivio, K. T. Butler, A. Walsh, M. Van Schilfgaarde, *Phys. Rev. B* **2014**, *89*, 155204.
[32] A. Sundqvist, O. J. Sa ndberg, M. Nyman, J.-H. Smått, R. Österbacka, *Adv. Energy Mater.* **2016**, *6*, 1502265.
[33] V. M. Le Corre, M. Stolterfoht, L. Perdigón Toro, M. Feuerstein, C. Wolff, L. Gil-Escrig, H. J. Bolink, D. Neher, L. J. A. Koster, *ACS Appl. Energy Mater.* **2019**, *2*, 6280.
[34] R. Kerremans, O. J. Sandberg, S. Meroni, T. Watson, A. Armin, P. Meredith, *Sol. RRL* **2020**, *4*, 1900221.
[35] P. Caprioglio, M. Stolterfoht, C. M. Wolff, T. Unold, B. Rech, S. Albrecht, D. Neher, *Adv. Energy Mater.* **2019**, *9*, 1901631.